Electronic Supplementary Material (ESI) for Physical Chemistry Chemical Physics.
This journal is © the Owner Societies 2016

Electronic Supplementary Information (ESI) for the article entitled:

Towards high-performance organic broadband photomemory transistors exhibiting remarkable UV-NIR response

Lili Du[1,+], Xiao Luo[1,+], Wenli Lv[1], Feiyu Zhao[1], Yingquan Peng[1,2,*] , Ying Tang[2] and Ying Wang[3]

[1] Institute of Microelectronics, School of Physical Science and Technology, Lanzhou University, South Tianshui Road 222#, Lanzhou 730000, China

[2] College of Optical and Electronic Technology, China Jiliang University, Xueyuan Street 258#, Hangzhou 310018, China

[3] College of Information Engineering, China Jiliang University, Xueyuan Street 258#, Hangzhou 310018, China

To whom correspondence and requests for materials should be addressed:
yqpeng@lzu.edu.cn (Y. Peng).

[+]These two authors equally contributed to this work (in no particular order).

1. Active material charge transport and optical absorption

In this paper, we present an ingenious and representative material design via sectional spectral cover from UV to NIR region, based on three types of materials below.

1.1 *Fullerene and its derivative*

Fullerene and its derivatives, a kind of near-spherical organic molecules with good structural stability, which can be easily deposited as thin films by various methods, have been extensively studied as *n*-type semiconducting materials to achieve a functional unit of an electronic device. In the past decades, such materials based on fullerene have been used in organic diodes, transistors, photovoltaics, catalyst, photodetectors due to its excellent electronic properties, including *n*-type behavior, a strong electron accepting nature, a high carrier mobility and superconductivity.[1] In

addition, density functional theory calculations by Marchiori *et al.*[2] anticipate a dipole assisted exciton dissociation at conjugated polymer/fullerene interface, suggesting fullerene is a promising material with the main features of high efficiency on charge separation.[3, 4]

Due to wide band gap, the fullerene and its derivatives exhibit strong absorption in the **UV-blue** spectral region, as shown in **Table S1**.

1.2 *Perylene bisimide derivative*

Perylene bisimide derivatives, most used as *n*-type semiconducting materials, have interesting transport and optical properties which stem from their strong tendency to form polycrystalline films in which the molecular planes orient in fixed directions with respect to the substrate. In the past decades, this type of material is used as molecule templating in organic solar cells[5], charge acceptor in photodetectors[6] and active layer in organic transistors[7] because of their interesting semiconductive properties. Furthermore, most perylene bisimide derivatives have a clear absorption between 450~550 nm, which is very suitable for **green** light absorption, as shown in Table S1.

Considering an ingenious design, in this paper, PTCDA is employed as green photoabsorber and sandwiched between C_{60} and PbPc because of its strong anisotropies in conduction (*p*-type *vs* *n*-type), depending upon whether conduction is measured perpendicular or parallel to the molecular plane.[8] In other words, PTCDA transports electrons in the directions parallel to the molecular planes and mainly holes in the direction perpendicular to the molecular planes, served as a transition layer between pn heterojunction (PbPc/C_{60}), which is beneficial to enhance exciton diffusion and dissociation.[6] In addition, it's also worth noting that heterojunctions based on thin films of PTCDA or its related bisimides, and certain phthalocyanines, show a marked tendency toward exciton dissociation at the phthalocyanines/PTCDA interface. These exciton dissociation processes are presumed to be assisted by the presence of fixed charges or high dipolar fields, as a result of charge transfer processes across the hetero-interface.[9]

1.3 *Phthalocyanine dyes*

Generally, most materials composed of phthalocyanine compounds are revealed to work as *p*-type semiconductors for OFET applications with only few phthalocyanine materials as *n*-type semiconductors and even less as ambipolar ones. Various functional phthalocyanines as well as their tetrapyrrole analogs, porphyrins, have been extensively studied as organic semiconductors since the first report of organic field effect transistors (OFETs) in 1986. The large conjugated system, excellent photoelectric characteristics, intriguing and unique optical properties, high thermal and chemical stability, and most importantly the easy functionalization of phthalocyanines render them ideal organic semiconductor materials as active layers for OFETs. Previous publications have indicated that the mobilities of phthalocyanine compounds are in the range of 10^{-4}~5 $cm^2V^{-1}s^{-1}$, even reaching up to 10 $cm^2V^{-1}s^{-1}$ for TiOPc-based OFET[10], which exceeds the mobility of amorphous silicon (a-Si) thin-film-transistors. The results indicate that phthalocyanine dyes can be a very good alternative to fabricate OFETs.

The spectra of phthalocyanine dyes consist of an intense absorption band in the visible region traditionally near 670nm called the Q band and a generally weaker band near 340 nm called the Soret or B band. The positions of the absorption bands in phthalocyanines, (particularly the Q band) are affected to a varying degree by the central metal, axial ligation, solvents, peripheral and nonperipheral substitution, aggregation, and by extension of the conjugation. Thus, the spectral absorption for some phthalocyanine molecule is highly redshifted and extended to NIR, covering **red-NIR** region, for example, lead phthalocynine (PbPc), tin phthalocyanine (SnPc), manganese phthalocyanine (MnPc), oxo-titanium phthalocyanine (TiOPc), chloroaluminum phthalocyanine (AlClPc), and so on, as shown in Table S1.

Table S1 Example illustrations of spectral absorption for fullerene and derivatives, perylene bisimide derivatives, and phthalocyanine dyes, respectively.

Materials		Photoabsorption region	Reference
	C_{60}	200-450 nm	R[11]
Fullerene and	C_{70}	200-600 nm	R[12]

derivatives	PCBM	200-500 nm	R[13]
	…	…	…
Perylene	PTCDA	400-600 nm	R[6]
bisimide	PTCDI	450-550 nm	R[14]
derivatives	PTCDI-PFDA	450-550 nm	R[15]
	…	…	…
	PbPc	600-900 nm	R[16]
	SnPc	600-900 nm	R[17]
Phthalocyanine	MnPc	650-850 nm	R[18]
dyes	TiOPc	600-900 nm	R[10]
	AlClPc	550-900 nm	R[19]
	…	…	…

2. Crystal and Morphological characterizations

Figure S1 shows the XRD pattern for PVA film prepared by 0.5 wt% concentration water solution. The diffraction pattern of as-prepared PVA indicates a diffraction band at $2\theta = 19.4^{o}$, which can be assigned to the partially crystalline nature of PVA polymer molecules as a result of strong intermolecular and intramolecular hydrogen bonding between the PVA chains[20]. The atomic force microscopy (AFM) image of PVA film corroborates the analysis results above, as shown in **Figure S2**a. It can be clearly observed that the PVA surface shows very small dots evenly distributed with their height being approximately 5 nm, which may be above-mentioned tiny crystals of PVA.[21] Furthermore, the 3D AFM image confirms that PVA layer was smooth and pinhole-free with its root-mean-square (RMS) roughness of ~1.2 nm.

In addition, in order to clarify the effect of charge-transport interface on the electrical properties of OFETs, morphologies of the C_{60} films are investigated in detail, as shown in Figure S2b-d. It is noted that the topography of C_{60} film on bare SiO_2 (Figure S2b) is extremely uniform and smooth with a RMS roughness of 1.58 nm. The needle-like small crystals with pores were present on the surface. Meanwhile, the morphology of C_{60} film on SiO_2/PVA substrate (Figure S2c) has a result similar to the case above with an RMS roughness of 2.40 nm. On the contrary, the morphology

of C_{60} deposited on SiO_2/PVA/OTS substrate (Figure S2d) shows drastic differences from the two cases above. Huge C_{60} crystalline grain is obtained. Previous studies have demonstrated that the OTS SAMs can improve the crystallinity of the organic semiconductors and the quality of the interface[22]. Thus, electrons can transport more easily. The results of output and transfer characteristics are also in consistence with the above-mentioned AFM images, as shown in **Figure S3** below.

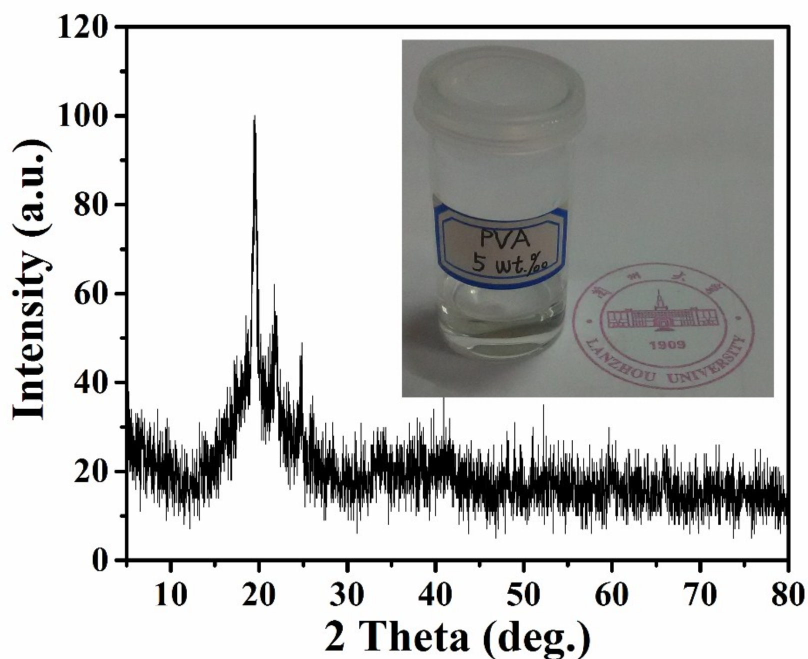

Figure S1. *XRD measurement of the as-prepared PVA film; the inset shows the 0.5 wt% PVA solution.*

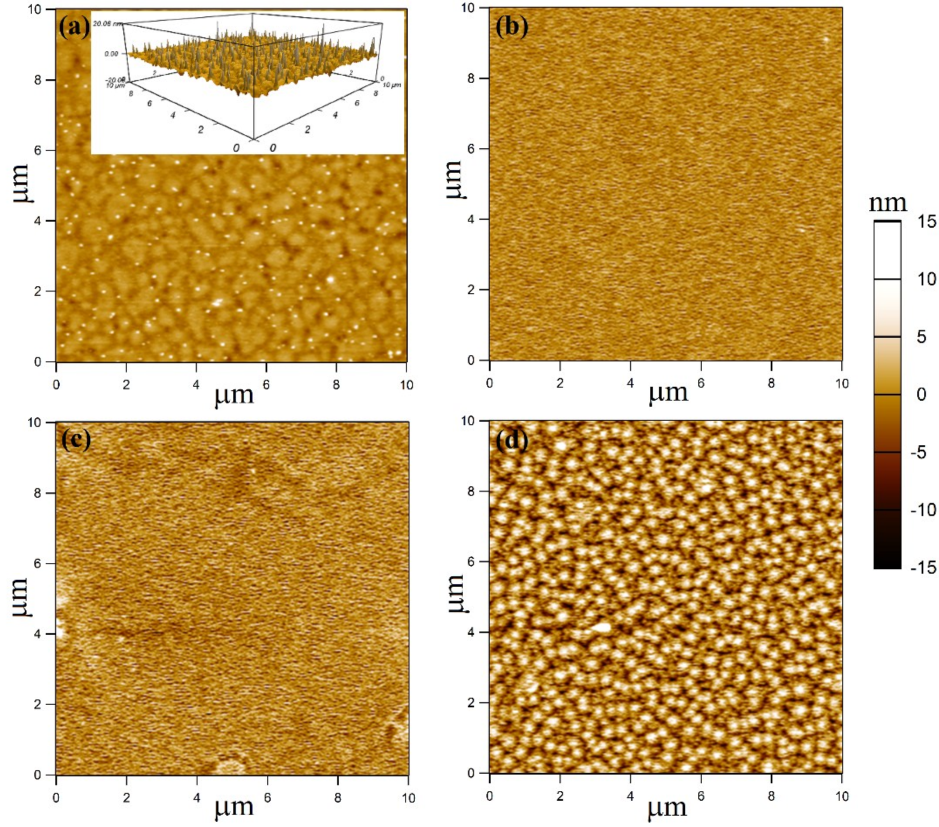

Figure S2. *(a) AFM image of the as-prepared PVA; the inset is corresponding 3D morphology. (b)-(d) are AFM images of C_{60} films deposited on different SiO_2 substrates: (b) bare SiO_2, (c) SiO_2/PVA, (d) SiO_2/PVA/OTS.*

3. Charge-carrier mobility and threshold voltage calculation

The field-effect mobility (μ_{FET}) is one of the most important parameters of organic field-effect transistor (OFET) devices, which is widely used to describe transport speed of the charge carrier in the FET device. A higher μ_{FET} provides a larger output current, shorter switching cycles, and a superior on/off ratio, which is also of significance for transistor-type memory. According to the gradual channel approximation, we obtained a typical drain current in the linear and saturation regime[23]:

$$I_{d,\mathrm{lin}} = \frac{W\mu_{lin}C_i}{L}[V_{ds}(V_{gs}-V_{\mathrm{T}})-\frac{V_{ds}^2}{2}],\ (V_{\mathrm{ds}} << (V_{\mathrm{gs}} - V_{\mathrm{T}})) \tag{1}$$

$$I_{d,sat} = \frac{W\mu_{sat}C_i}{2L}(V_{gs}-V_{\mathrm{T}})^2,\ (V_{\mathrm{ds}} > (V_{\mathrm{gs}} - V_{\mathrm{T}})), \tag{2}$$

where W and L are the channel width and length, C_i the insulator capacitance, μ_{lin} and μ_{sat} the field-effect mobility in the linear and saturation regimes, V_{gs} the gate voltage, V_{ds} the drain voltage and V_T the threshold voltage. In this paper, we extracted the μ_{sat} and V_T from the saturation transfer curve to characterize OFET mobility and memory window. Herein, the saturation mobility μ_{sat} and threshold voltage V_T were obtained by using the Equation (2) when the data were fitted to a quadratic function with the transfer curve in the saturation regime.

4. Electrical characteristics of related OFETs

Figure S3 shows the output and transfer characteristics of the pristine C_{60}-based field-effect transistor fabricated on different substrates, indicating typical n-channel operation. It can be obviously seen that the devices fabricated onto SiO_2/PVA/OTS substrate (Figure S3c-d) exhibit dramatically larger drain output current and on–off current ratio as compared with those fabricated onto bare SiO_2 (Figure S3c-d). A detailed summary including the key metrics for OFETs is presented in **Table S2**. The results above suggest that the as-proposed device structure with triple-layer coating of gate insulator is fundamental and promising for achieving high performance photomemory.

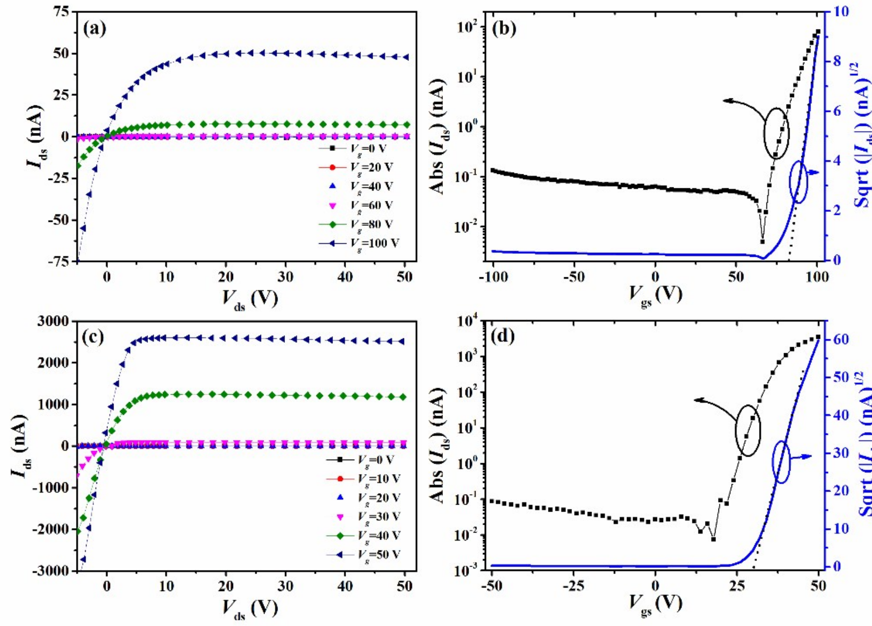

***Figure S3**. Output and transfer characteristics of the C_{60}-based field-effect transistors fabricated onto different substrates; (a)-(b): bare SiO_2; (c)-(d): SiO_2/PVA/OTS.*

Table S2. The summary of electrical parameters for the C_{60}-based OFETs.

Device structure [a]	μ_{sat} cm²/(V·s)	V_T V	S V/decade	I_{on}/I_{off}
SiO_2/C_{60}/Al	0.003	83	3.8	3×10^{3} [b]
SiO_2/PVA/OTS/C_{60}/Al	0.09	28	2.7	2×10^{5} [c]
This work	0.03	35	5.1	3×10^{4} [c]

[a] All the data listed for every device structure were the average values out of four samples;

[b] I_{on} were extracted in the saturation region of transistor operation at V_{ds}= 50 V, V_{gs}= 100 V, respectively;

[c] I_{on} were extracted in the saturation region of transistor operation at V_{ds}=V_{gs}= 50 V.

5. Photo memory characteristics of the as-prepared transistors

Figure S4 shows the transfer characteristics of the as-prepared organic photomemory under broadband illuminations with different radiation power, illustrating obvious photo memory properties from UV to NIR region. Furthermore, **Figure S5** shows a 3D memory window map of the organic photomemory transistor

under different wavelength and optical power, indicating that the memory property is broadband-responsive and it can be tuned by adjusting the incident optical power (P_{opt}), where an increasing P_{opt} can enhance total photon absorption, thereby increasing the optical memory window. Thus, it is concluded that higher memory window can be achieved under larger incident optical power. To prove the application of our device in photo memory further, the time-stability measurement of data retention capability is performed on the photomemory device after UV-NIR illuminations, as shown in **Figure S6**. The drain current I_{ds} can be almost maintained constant for ~100 s and has a slight decrease after 10^3 s for full spectral radiation. A small increase of I_{ds} after light-write process is attributed to the contribution of slow release of interfacial trapped charges under long time operation, indicating that the interfacial trap level is a shallow trap state. However, this current ratio is still recognizable for the photomemory device in a light-write/voltage-erase cycle. This result shows that the memory device with PVA electret is suitable for applying in photomemory. Besides, the memory window ΔV_T has a more or less decrease in 0~100 s range, which presumably stems from interfacial trap recombination, and then tends to hold stable after 100 s. Here, it is worthy of note that the photomemory efficiency, η, is still up to 50% after 10^3 s, indicating some potential applications in future broadband photomemory.

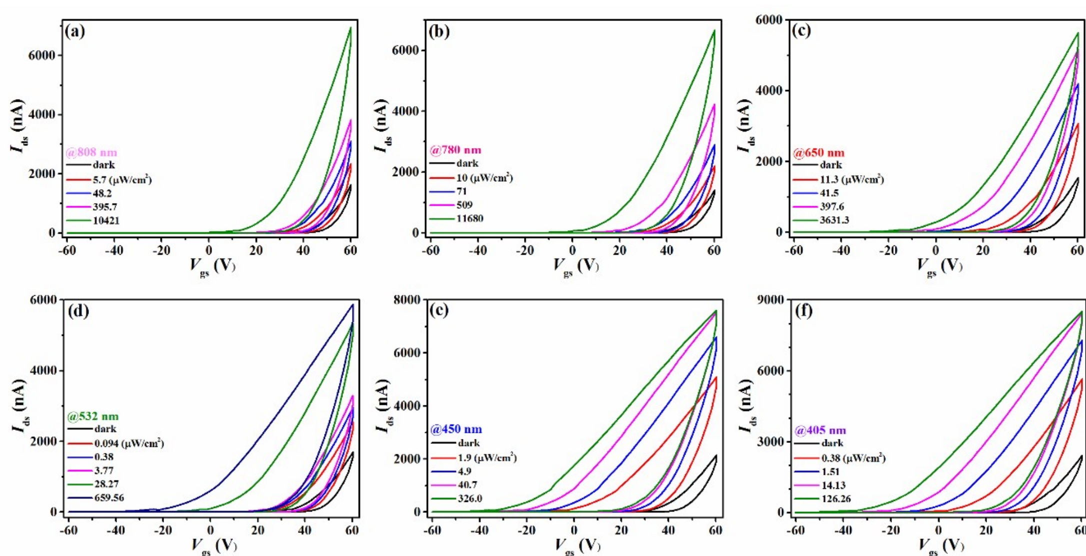

Figure S4. *Transfer characteristics of the organic photomemory under (a) 808 nm, (b)*

780nm, (c) 650nm, (d) 532nm, (e) 450nm and (f) 405nm illuminations with different radiation power, illustrating obvious photo memory properties from UV to NIR region.

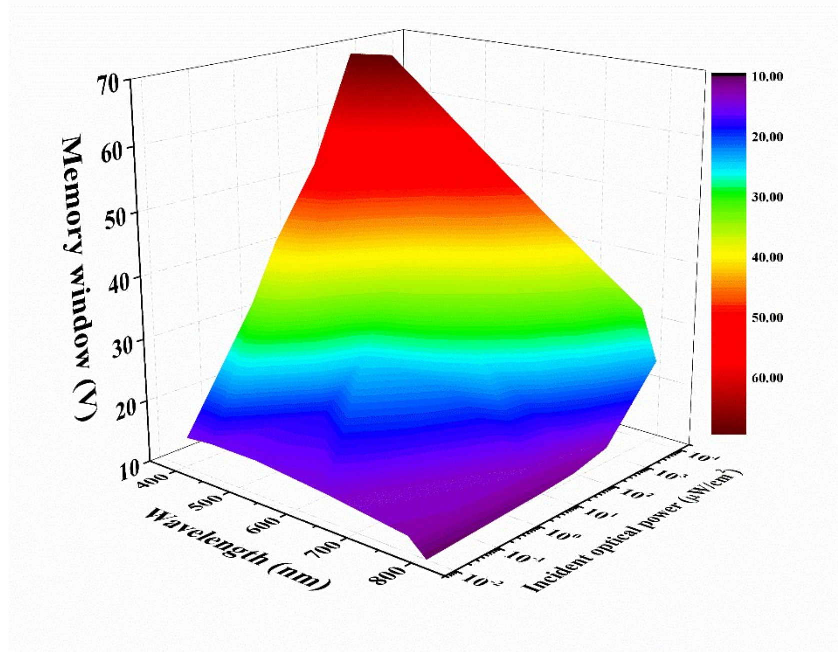

Figure S5. *3D memory window map of the organic broadband photomemory under different wavelength and optical power.*

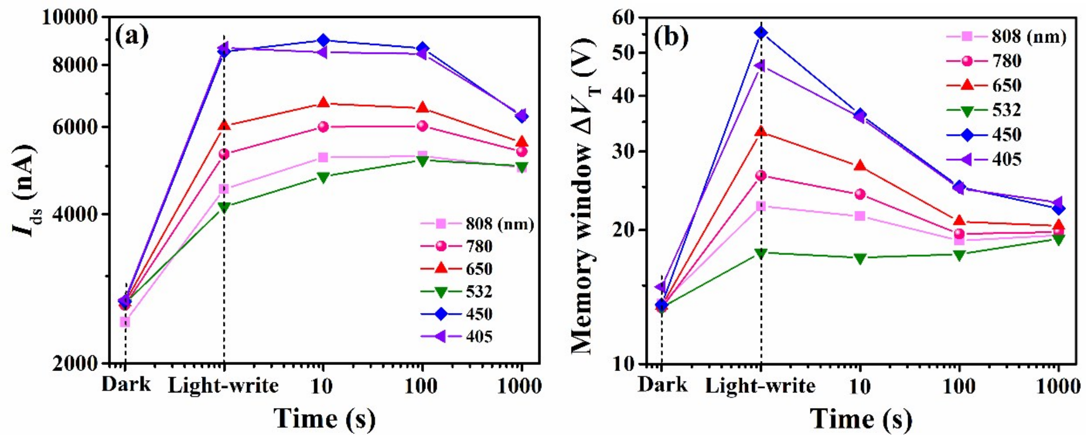

Figure S6. *Device time-stability measurement of the photo memory properties after light-write process. (a) drain current I_{ds} plotted as a function of time. (b) corresponding memory window ΔV_T plotted as a function of time.*

6. Estimation of energy barrier lowering for electron injection at source electrode

upon illumination, leading to photo multiplicative memory effect

1). The calculation process is as follows:

The image-force lowering of energy barrier at source-organic semiconductor contact, $\Delta\phi_{tot}$, can be calculated from the y-component of the electric field at the source contact[24] (y=0), $F_{y,0}$:

$$\Delta\phi_{tot} = q\sqrt{\frac{q\left|F_{y,0}\right|}{4\pi\varepsilon_r\varepsilon_0}} \tag{3}$$

As shown in **Figure S7**, a schematic illustration of carrier concentration is presented, as follows.

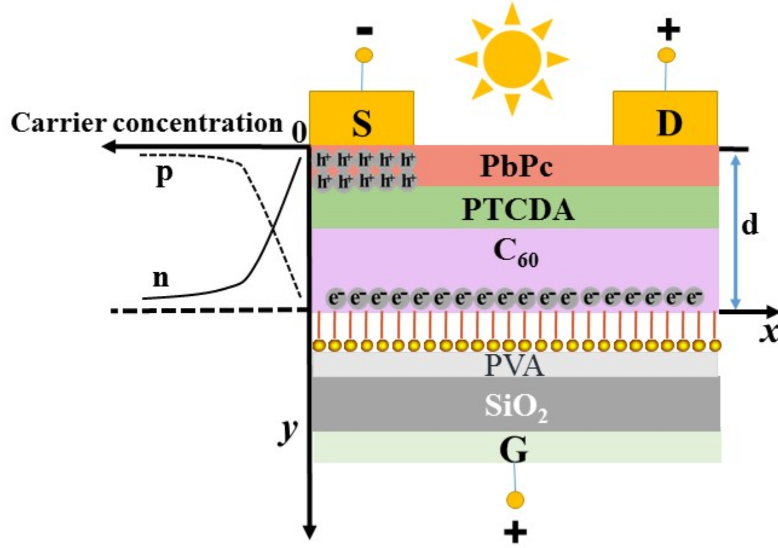

***Figure S7**. A schematic illustration of accumulation of photo generated holes (density p) near the source electrode and electrons (density n) near the gate dielectric in the channel layer.*

At V_g=0 and V_d=0, the y-component of the electric field near the source can be calculated by single carrier approximation[25] :

$$F_{y,0} = -\sqrt{\frac{2k_BTp_0}{\varepsilon_r\varepsilon_0}}. \tag{4}$$

Here p_0 is the hole concentration at y=0 under illumination, which can be expressed as $p_0=p_{0,g}+p_{0,ph}$, with $p_{0,g}$ the contribution from gate voltage and $p_{0,ph}$ from photo illumination . Substituting Equation (4) into (3), one obtains:

$$\Delta\phi_{tot} = q\left(\frac{q}{4\pi\varepsilon_r\varepsilon_0}\right)^{\frac{1}{2}}\left(\frac{2k_BTp_0}{\varepsilon_r\varepsilon_0}\right)^{\frac{1}{4}} \tag{5}$$

The hole concentration p_0 is related to the average hole density in the organic layer at x=0, p_a, that can be calculated from the threshold voltage[26], $V_{th,}$:

$$V_{th} = \frac{qp_a d}{c_i} \tag{6}$$

Here c_i is the gate capacitance per unit area. In order to get the relationship between p_0 and p_a, we assume: (i) y-component of electric field F_y is invariant of coordinate y; (ii) only holes are considered in calculating y-component of electric field. The equations describing hole concentration p, y-component of electric field F_y can be expressed as:

$$j_p = qp\mu_p F_y - qD_p\frac{dp}{dy} = 0 \quad \textit{(Balance of drift and diffusion of holes in y-direction.)} \tag{7}$$

$$\frac{dF_y}{dy} = \frac{q}{\varepsilon_0\varepsilon_r}p \quad \textit{(Poisson Equation)} \tag{8}$$

Here q is the elementary charge, μ_p the hole mobility and D_p the hole diffusion constant. The solution of above two equations is

$$p = p_0 e^{-\frac{\mu_p F_y}{D_p}y} \tag{9}$$

The average hole concentration at x=0, y=[0,d], p_a, is

$$p_a = \frac{1}{d}\int_0^d p_0 e^{-\frac{\mu_p F_y}{Dp}y}dy = \frac{k_BTp_0}{qF_yd}\left(1-e^{-\frac{qF_yd}{k_BT}}\right) \tag{10}$$

(*Einstein relation* $\mu_p/D_p=q/k_BT$ *is used*)

$$p_0 = \frac{qF_yd}{k_BT}\frac{p_a}{1-e^{-\frac{qF_yd}{k_BT}}} = \frac{qV_g}{k_BT}\frac{p_a}{1-e^{-\frac{qV_g}{k_BT}}} \quad (V_g = F_y\, d \text{ is used}) \tag{11}$$

For qV_g>>k_BT, above Equation is reduced to Equation (12)

$$p_0 = \frac{qV_g}{k_B T} p_a \tag{12}$$

Energy barrier lowering results from the holes which induced by the gate voltage, $\Delta\phi_g$, is

$$\Delta\phi_g = q\left(\frac{q}{4\pi\varepsilon_r\varepsilon_0}\right)^{\frac{1}{2}}\left(\frac{2k_B T p_{0,g}}{\varepsilon_r\varepsilon_0}\right)^{\frac{1}{4}} = q\left(\frac{q}{4\pi\varepsilon_r\varepsilon_0}\right)^{\frac{1}{2}}\left(\frac{2k_B T p_{a,g}}{\varepsilon_r\varepsilon_0}\frac{qV_g}{k_B T}\right)^{\frac{1}{4}} \tag{13}$$

Substituting Equation (6) into above Equation, we obtain:

$$\Delta\phi_g = q\left(\frac{q}{4\pi\varepsilon_r\varepsilon_0}\right)^{\frac{1}{2}}\left(\frac{2k_B T}{\varepsilon_r\varepsilon_0}\frac{c_i V_{th}}{qd}\frac{qV_g}{k_B T}\right)^{\frac{1}{4}} = q\left(\frac{q}{4\pi\varepsilon_r\varepsilon_0}\right)^{\frac{1}{2}}\left(\frac{2c_i V_{th}}{\varepsilon_r\varepsilon_0 d}V_g\right)^{\frac{1}{4}} \tag{14}$$

$p_{0,ph}$ can be calculated from the increment of average hole concentration $p_{a,ph}$ by illumination, which is related with the threshold voltage shift ΔV_{th} as follows:

$$\Delta V_{th} = \frac{qp_{a,ph}d}{c_i} \tag{15}$$

The total lowering of energy barrier by gate voltage and light illumination, $\Delta\phi_{tot}$, is

$$\Delta\phi_{tot} = \Delta\phi_g + \Delta\phi_{ph} = q\left(\frac{q}{4\pi\varepsilon_r\varepsilon_0}\right)^{\frac{1}{2}}\left(\frac{2k_B T(p_{0,g}+p_{0,ph})}{\varepsilon_r\varepsilon_0}\right)^{\frac{1}{4}}$$
$$= q\left(\frac{q}{4\pi\varepsilon_r\varepsilon_0}\right)^{\frac{1}{2}}\left(\frac{2c_i(V_{th}+\Delta V_{th})}{\varepsilon_r\varepsilon_0 d}V_g\right)^{\frac{1}{4}} \tag{16}$$

The net energy barrier lowering induced by light illumination is

$$\Delta\phi_{ph} = \Delta\phi_{tot} - \Delta\phi_g . \tag{17}$$

Then, we obtained the $\Delta\phi_{tot}$ ~0.476 eV, and $\Delta\phi_{ph}$ ~0.139 eV at V_g=60 V under 405 nm illumination.

2). According to the thermionic emission theory[27], the injected current at source electrode can be expressed as:

$$J_{th} \sim F_{y,0} e^{\sqrt{F_{y,0}}} e^{-\frac{\phi}{k_B T}} \tag{18}$$

The barrier lowering $\Delta\phi_{ph}$~0.139eV. If $F_{y,0}$ is a constant, we estimate the $\Delta J_{th} / J_{th}$ is about

$$e^{\frac{\Delta\phi_{ph}}{k_B T}} = e^{\frac{0.139eV}{0.0259eV}} \approx 214 \tag{19}$$

Actually, the concentration of electrons at y=0 will increase when injection barrier is lowered under illumination, and $F_{y,0}$ will be decreased. Thus, the increment of the injected current under illumination, $\Delta J_{th} / J_{th}$, should be smaller than 214 times. The multiplication effect of ~10^2 magnitude is noteworthy, which indicates that photoinduced charge-injection enhancement is non-negligible and photo multiplicative memory effect indeed exists under a certain voltage offset, as schematically shown in **Figure S8**.

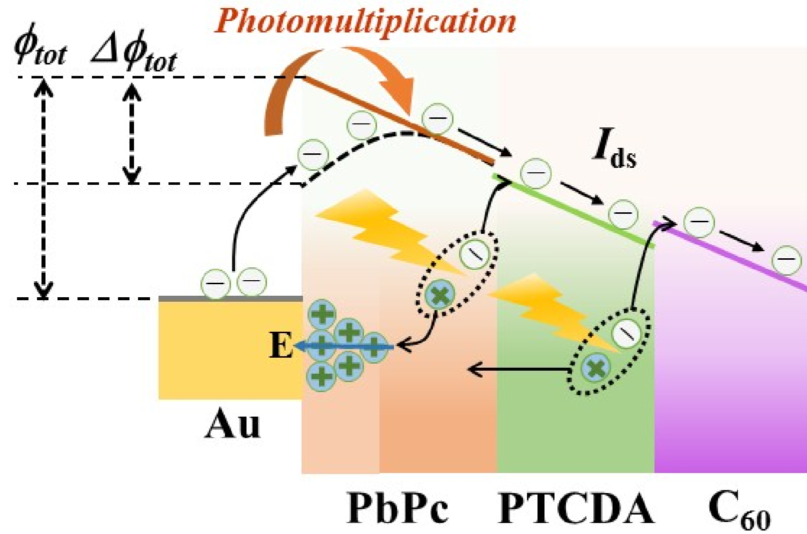

Figure S8*. Schematic energy level diagram for photoinduced charge-injection enhancement kinetics, leading to photo multiplicative memory effect.*

7. Effect of mobility imbalance of the three materials on the device properties

According to previous publications, the three materials used in the experiment

have imbalanced mobilities. For comparison, C_{60} as n-type semiconductor has an electron mobility of 10^{-2}~10^{-1} $cm^2V^{-1}s^{-1}$; PbPc as p-type semiconductor has a hole mobility of ~10^{-5} $cm^2V^{-1}s^{-1}$; and PTCDA is a weak p-type material with a mobility range of 10^{-7}~1.4 $cm^2V^{-1}s^{-1}$, depending on material purity and the conditions of film deposition[28]. As a result, the effect of the materials' mobility imbalance on the device properties are mainly reflected in the below aspects:

(a) C_{60} is firstly used as a photo absorbing material for UV-blue region due to its wide band gap. More importantly, it also serves as charge-carrier transport layer close to the surface of gate dielectric because of its higher mobility. Thus, photogenerted- and electrically-injected charges will achieve faster transport and extraction, thereby improving device properties.

(b) In this experiment, we design an electron energy-level mismatch between the gold electrode and PbPc molecule to suppress output signal in darkness, which is advantageous to enhance the photomemory efficiency. Furthermore, under illumination, smaller hole mobility of PbPc will be beneficial to induce high-density accumulated holes near source electrode, leading to energy-level bend downwards and then triggering electron injection enhancement effect, eventually further improving photomemory efficiency (details see main body of manuscript and section 6 above).

Reference

1. R. Saran, M. N. Nordin and R. J. Curry, *Advanced Functional Materials*, 2013, **23**, 4149-4155.
2. C. Marchiori and M. Koehler, *Synthetic Metals*, 2010, **160**, 643-650.
3. H. Tamura, I. Burghardt and M. Tsukada, *The Journal of Physical Chemistry C*, 2011, **115**, 10205-10210.
4. H. Tamura and I. Burghardt, *Journal of the American Chemical Society*, 2013, **135**, 16364-16367.
5. P. Sullivan, T. S. Jones, A. Ferguson and S. Heutz, *Applied Physics Letters*, 2007, **91**, 233114.
6. Y. Peng, W. Lv, B. Yao, G. Fan, D. Chen, P. Gao, M. Zhou and Y. Wang, *Organic Electronics*, 2013, **14**, 1045-1051.
7. M. M. Ling, P. Erk, M. Gomez, M. Koenemann, J. Locklin and Z. Bao,

Advanced materials, 2007, **19**, 1123-1127.
8. J. Ostrick, A. Dodabalapur, L. Torsi, A. Lovinger, E. Kwock, T. Miller, M. Galvin, M. Berggren and H. Katz, *Journal of Applied Physics*, 1997, **81**, 6804-6808.
9. R. Schlaf, B. Parkinson, P. Lee, K. Nebesny and N. Armstrong, *The Journal of Physical Chemistry B*, 1999, **103**, 2984-2992.
10. L. Li, Q. Tang, H. Li, X. Yang, W. Hu, Y. Song, Z. Shuai, W. Xu, Y. Liu and D. Zhu, *Advanced materials*, 2007, **19**, 2613-2617.
11. A. Hebard, R. Haddon, R. Fleming and A. Kortan, *Applied physics letters*, 1991, **59**, 2109-2111.
12. S. Pfuetzner, J. Meiss, A. Petrich, M. Riede and K. Leo, *Applied Physics Letters*, 2009, **94**, 223307.
13. P. H. Wöbkenberg, D. D. Bradley, D. Kronholm, J. C. Hummelen, D. M. de Leeuw, M. Cölle and T. D. Anthopoulos, *Synthetic Metals*, 2008, **158**, 468-472.
14. A. L. Briseno, S. C. Mannsfeld, C. Reese, J. M. Hancock, Y. Xiong, S. A. Jenekhe, Z. Bao and Y. Xia, *Nano letters*, 2007, **7**, 2847-2853.
15. M. R. Raj, S. Anandan, R. V. Solomon, P. Venuvanalingam, S. S. K. Iyer and M. Ashokkumar, *Journal of Photochemistry and Photobiology A: Chemistry*, 2012, **247**, 52-62.
16. Y. Li, W. Lv, X. Luo, L. Sun, F. Zhao, J. Zhang, J. Zhong, F. Huang and Y. Peng, *Organic Electronics*, 2015, **26**, 186-190.
17. M. El-Nahass and S. Yaghmour, *Applied Surface Science*, 2008, **255**, 1631-1636.
18. A. Günsel, M. Kandaz, F. Yakuphanoglu and W. Farooq, *Synthetic Metals*, 2011, **161**, 1477-1482.
19. J. Cao, J.-Z. Sun, J. Hong, X.-G. Yang, H.-Z. Chen and M. Wang, *Applied physics letters*, 2003, **83**, 1896-1898.
20. A. Gautam and S. Ram, *Materials Chemistry and Physics*, 2010, **119**, 266-271.
21. W. Wang, S. K. Hwang, K. L. Kim, J. H. Lee, S. M. Cho and C. Park, *ACS applied materials & interfaces*, 2015, **7**, 10957-10965.
22. M. Shtein, J. Mapel, J. B. Benziger and S. R. Forrest, *Applied Physics Letters*, 2002, **81**, 268-270.
23. Z. Bao and J. Locklin, *Organic field-effect transistors*, CRC press, 2007.
24. S. M. Sze and K. K. Ng, *Physics of semiconductor devices*, John Wiley & Sons, 2006.
25. Y.-q. Peng, W.-m. Meng, R.-s. Wang, C.-z. Ma, X.-s. Li, H.-w. Xie, R.-h. Li, M. Zhao, J.-t. Yuan and Y. Wang, *Applied Surface Science*, 2009, **255**, 8010-8013.
26. S. Okur, F. Yakuphanoglu and E. Stathatos, *Microelectronic Engineering*, 2010, **87**, 635-640.
27. Y. Peng and J. Yang, *Appl. Phys. A*, 2005, **80**, 1511-1516.
28. S. R. Forrest, M. L. Kaplan and P. H. Schmidt, *Journal of Applied Physics*, 1984, **55**, 1492-1507.